International Journal of Coal Geology 86 (2011) 213–221

Contents lists available at ScienceDirect

International Journal of Coal Geology

journal homepage: www.elsevier.com/locate/ijcoalgeo

A model of coal–gas interaction under variable temperatures

W.C. Zhu [a,*], C.H. Wei [a], J. Liu [b,c], H.Y. Qu [b], D. Elsworth [d]

[a] Center for Rock Instability and Seismicity Research, Northeastern University, Shenyang, 110004, China
[b] School of Mechanical Engineering, University of Western Australia, Crawley, 6009 WA, Australia
[c] State Key Laboratory for Geomechanics and Deep Underground Engineering, China University of Mining and Technology, Beijing, 100083, China
[d] Department of Energy and Mineral Engineering, Penn State University, University Park, PA, USA

ARTICLE INFO

Article history:
Received 2 September 2010
Received in revised form 30 January 2011
Accepted 31 January 2011
Available online 9 March 2011

Keywords:
Gas flow
Coal–gas interaction
Variable temperatures
Thermal convection
Numerical simulation

ABSTRACT

Although coal–gas interactions have been comprehensively investigated, fewer studies consider the impact of thermal effects. In this study, a fully coupled model of coal deformation, gas transport, and thermal transport is developed and solved using the finite element method. A general model is developed to describe the evolution of coal porosity under the combined influence of gas pressure, thermally induced solid deformation, thermally induced gas adsorption change, and gas-desorption-induced solid deformation. This porosity-evolution relationship is implemented into a fully coupled model for coal deformation, gas transport, and thermal transport using the finite element (FE) model. The FE model represents important nonlinear responses due to the effective stress effects that cannot be recovered where mechanical influences are not rigorously coupled with the gas and the thermal transport systems. The controlling effects of gas pressure, temperature and gas sorption on these nonlinear responses of coal porosity and permeability to gas production are quantified through a series of simulations. It is found that the gas-desorption-induced deformation is the most important factor that controls these nonlinear responses. In this work, among the factors such as thermal expansion of solid and gas, and convective heat flux, in addition to the thermal diffusion, the heat sink due to thermal dilatation of gas is most prominent factor in altering the temperature of coal seam. This conclusion demonstrates that the thermal impact on coal–gas interactions cannot be neglected especially where the temperature is high.

1. Introduction

Advances in our understanding of coal–gas interactions have changed the manner in which we treat coalbed methane: from mitigating its dangers as a mining hazard to developing its potential as an unconventional gas resource recovered as a useful by-product of CO_2 sequestration. Coal deposits contain gases (mostly methane) in significant quantities which may be recovered by desorption and subsequent transport in cleats to satisfy safety needs in mining, recovery of methane as an energy resource or as a sequestration target for the disposal of carbon dioxide. Gas migration in coal seams is one of the most important factors that result in coal and gas outbursts (Litwiniszyn, 1985; Lama and Bodziony, 1998). In this regard, improved solutions, including the prediction of gas emission, the design of the most suitable panel and pre-drainage systems, further optimization of post-drainage systems and other methods for the control of gas emissions during mining operations are essential to predict and prevent the coal and gas outbursts (Noack, 1998). Coalbed methane is also a significant natural energy resource although effective recovery requires that the coal permeability is sufficiently high to allow effective recovery. This is not always the case, as in China where permeability is often too low (Scott, 2002) and methods of permeability enhancement must be considered, either through stimulation or as a natural consequence of methane recovery and related coal shrinkage and permeability augmentation (Creedy, 1991).

From the 1970s onwards there has been a growing interest in the production of coalbed methane as a fuel. This has now evolved from a little-known resource with high operational costs to a competitive mainstream natural gas resource (Ayers, 2002). At the end of the 1980s, this industry searched for methods to enhance production. The successes of Enhanced Oil Recovery (EOR) gave the coalbed methane industry the idea that gas injection could also be successfully applied in unmineable coalbeds to enhance coalbed methane (ECBM) recovery (van Bergen et al., 2006). Two main benefits can be obtained from ECBM that includes the injection of a displacing gas. One is to increase production rates of methane and to thereby shorten the time to return on investment; the other is to mitigate increasing concentrations of carbon dioxide in the atmosphere to thereby reduce effects of global climate change (Gunter et al., 1997; Metz, 2005; Reichle et al., 1999).

When coal is recovered by mining, or fluid recovered or injected, the geothermal equilibrium in the subsurface system is disturbed. As a

* Corresponding author. Tel.: +86 24 83687705; fax: +86 24 83671626.
E-mail address: zhuwancheng@mail.neu.edu.cn (W.C. Zhu).

0166-5162/$ – see front matter © 2011 Elsevier B.V. All rights reserved.
doi:10.1016/j.coal.2011.01.011

result of this disturbance, complex interactions of stress and physical chemistry are affected by thermal transport (e.g., Han et al., 2010). Quantification of this interaction between coal and gas, particularly with the influence of production-induced temperature changes, defines the objective of this study.

1.1. Factors affecting coal seam permeability

Gas migration in coal seams is a process associated with coal seam deformation, gas slippage and absorption-induced matrix shrinkage of coal, as well as thermal transfer. To properly account for the response, these coupled processes bust be evaluated together, to evaluate appropriate feedbacks within this complex and interactive system. This problem is complex because the related physical processes are at PVT (pressure, volume and temperature) conditions where feedbacks between physical process and activation of chemical effects are strong and nonlinear. There are a variety of interactive effects.

Effective stress is the first and probably most important factor that influences the evolution of gas permeability in coal seams. An increase in gas pressure results in a decrease in effective stress, which in turn results in the dilation of coal cleats and in a concomitant increase in coal permeability (Zhu et al., 2007). Second, gas slippage and coal matrix shrinkage have significant influences on the permeability of coal. However, this feedback is complex, and increases in pressure also induce swelling and may cause a reduction in permeability (Izadi et al., 2011)—the behaviors are complex. Gas slippage (Klinkenberg) effects are shown to be significant (Harpalani and Schraufnagel, 1990; Harpalani and Chen, 1997) as are the influences of elastic and swelling-induced dilation on permeability (Shi and Durucan, 2001). This is exacerbated in the presence of fluids such as CO_2 with a preferential affinity over methane for the coal media. With regard to CO_2 injection for ECBM recovery and CO_2 sequestration in coalbeds, volumetric strain due to CO_2 sorption in coal seam was at least 1.5 times higher than from methane. In this respect differential swelling as a result of CO_2 injection can also cause profound changes in fracture porosity and permeability with significant implication for ECBM recovery (Mazumder and Wolf, 2008). Finally, temperature is also a key factor controlling coal deformation and gas migrations especially when underground mining and coal seam gas exploration goes deeper.

1.2. Thermal effect on the gas flow

Geothermal gradients in the subsurface sometimes exceed the normal 25 °C/km resulting in potentially high temperatures at shallow depths. Temperature is a key factor in modulating deformation and gas migration in coal. First, the thermal stress at depth may change the in situ stress conditions thereby altering permeability. Second, the PVT conditions of coalbed gas are sensitive to the in-situ temperature. And third, and most importantly, temperature is a key factor controlling the absorption or adsorption and related desorption of gas to the coal seam.

High temperature favors the existence of gas in a free state rather than as sorbed to the matrix. At higher temperatures the Langmuir constant decreases, resulting in a lower initial slope of the isotherm (Bustin and Clarkson, 1998). Levy et al. (1997) found that for Australian coals a linear decrease in methane adsorption capacity of 0.12 m^3/ton per 1 °C-increase in temperature occurs over a temperature range of 20–65 °C at a pressure of 5 MPa. If the entire coal surface was homogeneous such that each potential sorption site had the same heat of adsorption, then the Langmuir volume would be the same regardless of temperature (Brunauer, 1943). However, sorption capacity decreases with an increase temperature, indicating that the geometry and number of potential sorption sites also changes with temperature. This explains why coal sorption isotherms change shape with increasing temperature; in general, the Langmuir volume decreases and the Langmuir pressure increases (Scott, 2002).

Successful prediction of the response of coal seams to production relies on understanding the interaction of these complex factors. The potentially strong feedbacks between processes results in modeling being the only practical method of following the response. Currently, most models have ignored the influence of temperature on the response of the coal seams to gas recovery. In this study, we define this chain of reactions, trigged by coal mining, coalbed extraction, or CO_2 injection, as "coupled multiphysics" implying that one physical process affects the initiation and progress of another. The individual processes, in the absence of full consideration of cross couplings, form the basis of very well-known disciplines such as elasticity, hydrology and heat transfer. Therefore, the inclusion of cross couplings is the key to rigorously formulate the coupled multiphysics of coal–gas interactions. Here we develop new cross coupling relations between coal porosity and mechanical, hydrological, chemical and thermal volumetric strains under conditions of variable stress. The cubic relation between porosity and permeability is then introduced to relate coal storage capability (changing porosity) to coal transport characteristics (changing permeability) also under conditions of variable stress. These two relations are the key cross couplings that couple the multiphysics of coal–gas interactions under variable temperatures.

2. Governing equations

We develop the mathematical representation for the coupled thermal transport, gas flow and geomechanical response to gas flow in coal. Necessary relations include the enforcement of conservation of momentum, mass and energy with appropriate constitutive laws for fluid and heat transport and for stress and deformation. There is no explicit representation in the model of any additional fracturing because the formulations are based on a representative element volume (REV) within the coal seam.

2.1. Mechanical equilibrium

The coal seam is assumed to behave as a linear elastic medium relative to anticipated changes in stress, as induced by methane production. Temperature changes may induce changes in porosity, which is directly analogous to matrix shrinkage in coalbeds where porosity increases as gas desorbs during drawdown (Palmer and Mansoori, 1996). The sorption-induced strain is approximated by treating the swelling/shrinkage of the coal matrix as equivalent to thermal contraction/expansion. In this regard, the constitutive relations for a nonisothermal gas-desorbing coalbed can be expressed in terms of the total stress σ_{ij} (positive for tension), strain ε_{ij}, pore gas pressure p (negative for suction), temperature change T, and volumetric matrix shrinkage strain ε_s induced by gas desorption from coal as

$$\sigma_{ij} = 2G\varepsilon_{ij} + \frac{2G\nu}{1-2\nu}\varepsilon_{kk}\delta_{ij} - \alpha p\delta_{ij} - K\alpha_T T\delta_{ij} - K\varepsilon_s\delta_{ij}, \quad (1)$$

in which G is the shear modulus (Pa), ν is the drained Poisson's ratio, δ_{ij} is the Kronecker delta defined as 1 for $i=j$ and 0 for $i\neq j$, $K\,(=2G(1+\nu)/3(1-2\nu)=E/3(1-2\nu))$ is the drained bulk modulus of the medium, α_T is the coefficient of volumetric expansion of the bulk medium under constant pore pressure and stress (K^{-1}), and the parameter $\alpha(\leq 1)$ is Biot's coefficient, which depends on the compressibility of the constituents and can be defined as

$$\alpha = 1 - \frac{K}{K_s}, \quad (2)$$

where K_s is the effective bulk modulus of the solid constituent (Pa), and the effective stress is defined as $\sigma'_{ij}=\sigma_{ij}+\alpha p\delta_{ij}$.

The macroscopic volumetric matrix shrinkage strain ε_s induced by gas desorption from coal is assumed to be proportional to the content of absorbed gas as (Cui and Bustin, 2005; Durucan et al., 2005)

$$\varepsilon_s = \alpha_{sg} V_{sg}, \tag{3}$$

where V_{sg} is the content ($m^3 \cdot kg^{-1}$) of absorbed gas (see Eq. (10)) and α_{sg} is the coefficient of sorption-induced volumetric strain (kg m^{-3}).

Based on Eq. (1), the volume strain is

$$\varepsilon_v = \frac{1}{K}(\overline{\sigma} + \alpha p) + \alpha_T T + \varepsilon_s, \tag{4}$$

where $\varepsilon_v=\varepsilon_1+\varepsilon_2+\varepsilon_3$ is the volumetric strain of the coal matrix and $\overline{\sigma} = \frac{1}{3}(\sigma_1 + \sigma_2 + \sigma_3)$ is the mean stress.

Using compact notation, the equations of equilibrium and the strain-displacement relations can be expressed as

$$\sigma_{ij,j} + F_i = 0 \tag{5}$$

and

$$\varepsilon_{ij} = \frac{1}{2}\left(u_{i,j} + u_{j,i}\right), \tag{6}$$

respectively, where F_i and u_i ($i=x,y,z$) are the components of the net body force and displacement in the i-direction. Based on Eqs. (1) and (6), a modified Navier equation may be derived via Eq. (5), in terms of displacement under a combination of changes of applied stresses, pore gas pressures, and temperature as

$$Gu_{i,jj} + \frac{G}{1-2\nu}u_{j,ji} - \alpha p_{,i} - K\alpha_T T_{,i} - K\varepsilon_{s,i} + F_i = 0. \tag{7}$$

In the absence of pore gas pressure, temperature gradients and desorption-induced matrix shrinkage strain ε_s, Eq. (7) reduces to the classical Navier equations for an ideal elastic solid.

2.2. Gas flow

The coal seam is composed of a solid matrix that contains interstitial pore space filled with a freely diffusing pore gas. The absorption or desorption of gas may occur when the gas pressure and porosity of the coal seam are changed.

Gas flow in a porous medium is governed by a mass balance equation

$$\frac{\partial m}{\partial t} + \nabla\cdot\left(\rho_g \mathbf{q}_g\right) = Q_s, \tag{8}$$

where ρ_g is the gas density ($kg \cdot m^{-3}$), $\mathbf{q}_g$ is the Darcy velocity of the gas phase ($m \cdot s^{-1}$), Q_s is a source term ($kg \cdot m^{-3} \cdot s^{-1}$) related to injection through local injection/production wells, t is the time (s), and m is the methane content ($kg \cdot m^{-3}$), including free-phase gas and absorbed gas, and is defined as

$$m = \phi\rho_g + \rho_{ga}\rho_c V_{sg} \tag{9}$$

where ϕ is the porosity, ρ_{ga} is the gas density at standard conditions ($kg \cdot m^{-3}$), ρ_c is the coal density ($kg \cdot m^{-3}$) and V_{sg} is the content ($m^3 \cdot kg^{-1}$) of absorbed gas. The first and second terms on the right-hand side of Eq. (9) represent the content of free-phase gas and absorbed gas, respectively.

Based on the Langmuir isotherm under different temperature, the gas absorption volume V_{sg} is defined as (Liang, 2000)

$$V_{sg} = \frac{V_L p}{p + P_L}\ exp\left[-\frac{c_2}{1 + c_1 p}(T_{ar} + T - T_t)\right], \tag{10}$$

where V_L and P_L represent the Langmuir volume constant ($m^3 \cdot kg^{-1}$) and Langmuir pressure constant (Pa) at temperature T_t, respectively, where T_{ar} is the absolute reference temperature in the stress-free state (K), T_t is the reference temperature for the desorption/adsorption test of gas (K), $(T_{ar}+T)$ is the temperature of the coal seam (K), c_1 is the pressure coefficient (Pa^{-1}), and c_2 is the temperature coefficient (K^{-1}).

The ideal gas law is used to describe the relation between gas density, gas pressure and temperature as

$$\rho_g = \frac{M_g}{R(T_{ar} + T)}p, \tag{11}$$

where ρ_g is the gas density ($kg \cdot m^{-3}$), p is the gas pressure (Pa), M_g is the molecular weight of the gas ($kg \cdot mol^{-1}$), R is the universal gas constant ($J \cdot mol^{-1} \cdot K^{-1}$) and T_{ar} is the absolute reference temperature in the stress-free state (K).

Based on Eq. (11), the gas density at standard condition ρ_{ga} can be expressed as

$$\rho_{ga} = \frac{M_g p_a}{RT_a}, \tag{12}$$

where p_a and T_a are the pressure (Pa) and temperature (K) of gas at standard conditions.

Assuming that the effect of gravity is small in comparison to the induced pressure gradient, the Darcy velocity, $\mathbf{q}_g$, is given by

$$\mathbf{q}_g = -\frac{k}{\mu}\nabla p \tag{13}$$

where k is the permeability of the coal (m^2) and μ is the dynamic viscosity of the gas (Pa·s). Substituting Eqs. (9)–(13) into Eq. (8), we obtain

$$\begin{aligned}
&\frac{\partial\phi}{\partial t}\frac{1}{(T_{ar}+T)}p + \phi\frac{1}{(T_{ar}+T)}\frac{\partial p}{\partial t} - \phi p\frac{1}{(T_{ar}+T)^2}\frac{\partial T}{\partial t} \\
&+ \frac{p_a\rho_c V_L}{T_a}\left\{\begin{array}{l}
\frac{P_L}{(p+P_L)^2}\exp\left(-\frac{c_2}{1+c_1 p}(T+T_{ar}-T_t)\right)\frac{\partial p}{\partial t} \\
+\frac{p}{(p+P_L)}\exp\left(-\frac{c_2}{1+c_1 p}(T+T_{ar}-T_t)\right)\times\frac{c_1 c_2}{(1+c_1 p)^2}(T+T_{ar}-T_t)\frac{\partial p}{\partial t} \\
-\frac{p}{(p+P_L)}\exp\left(-\frac{c_2}{1+c_1 p}(T+T_{ar}-T_t)\right)\times\frac{c_2}{1+c_1 p}\frac{\partial T}{\partial t}
\end{array}\right\} \\
&-\frac{1}{\mu}\left[\frac{\partial}{\partial x}\left(\frac{pk}{(T_{ar}+T)}\frac{\partial p}{\partial x}\right) + \frac{\partial}{\partial y}\left(\frac{pk}{(T_{ar}+T)}\frac{\partial p}{\partial y}\right)\right] = Q_s.
\end{aligned} \tag{14}$$

As previously defined (Zhang et al., 2008; Detournay and Cheng, 1993; Cui and Bustin, 2005), the general porosity model is expressed as

$$d\phi = \frac{1}{K}(\alpha - \phi)(d\overline{\sigma} + dp). \tag{15}$$

Considering the initial state with a mean compressive stress within the coal seam of $\overline{\sigma}_0$, the pore pressure of p_0, and the porosity of ϕ_0, the integration of Eq. (15) yields

$$\int_{\phi_0}^{\phi}\frac{d\phi}{\alpha-\phi} = \frac{1}{K}\left(\int_{\overline{\sigma}_0}^{\overline{\sigma}} d\overline{\sigma} + \int_{p_0}^{p} dp\right), \tag{16}$$

and

$$\phi = \alpha - (\alpha - \phi_0)\ exp\left\{-\frac{1}{K}\left[(\overline{\sigma} - \overline{\sigma}_0) + (p - p_0)\right]\right\}. \tag{17}$$

Substituting Eq. (4) into Eq. (17) yields

$$\phi = \alpha-(\alpha-\phi_0)\ exp\left\{-\left[\left(\varepsilon_v + \frac{p}{K_s}-\varepsilon_s-\alpha_T T\right)-\left(\varepsilon_{v0} + \frac{p_0}{K_s}-\varepsilon_{s0}-\alpha_T T_0\right)\right]\right\}, \tag{18}$$

where the subscript '0' denotes the initial value of the corresponding variables.

Based on Eq. (18), the differentiation of ϕ with respect to t results in

$$\begin{aligned}\frac{\partial\phi}{\partial t} &= -(\alpha-\phi_0)\ exp\left\{-\left[\left(\varepsilon_v + \frac{p}{K_s}-\varepsilon_s-\alpha_T T\right)-\left(\varepsilon_{v0} + \frac{p_0}{K_s}-\varepsilon_{s0}-\alpha_T T_0\right)\right]\right\}\\ &\quad\times\left[-\left(\frac{\partial\varepsilon_v}{\partial t} + \frac{1}{K_s}\frac{\partial p}{\partial t}-\frac{\partial\varepsilon_s}{\partial t}-\alpha_T\frac{\partial T}{\partial t}\right)\right],\\ &= -(\alpha-\phi)\times\left[-\left(\frac{\partial\varepsilon_v}{\partial t} + \frac{1}{K_s}\frac{\partial p}{\partial t}-\frac{\partial\varepsilon_s}{\partial t}-\alpha_T\frac{\partial T}{\partial t}\right)\right]\end{aligned} \tag{19}$$

where $\frac{\partial\varepsilon_s}{\partial t}$ can be expressed as follows when substituting Eq. (10) into Eq. (3):

$$\frac{\partial\varepsilon_s}{\partial t} = \alpha_{sg}V_L\times\left[\begin{array}{l}\frac{P_L}{(p+P_L)^2}\exp\left(-\frac{c_2}{1+c_1p}(T+T_{ar}-T_t)\right)\frac{\partial p}{\partial t}\\ +\frac{p}{(p+P_L)}\exp\left(-\frac{c_2}{1+c_1p}(T+T_{ar}-T_t)\right)\times\frac{c_1c_2}{(1+c_1p)^2}(T+T_{ar}-T_t)\frac{\partial p}{\partial t}\\ -\frac{p}{(p+P_L)}\exp\left(-\frac{c_2}{1+c_1p}(T+T_{ar}-T_t)\right)\times\frac{c_2}{1+c_1p}\frac{\partial T}{\partial t}\end{array}\right]. \tag{20}$$

In addition, the coal permeability is assumed to vary with porosity as

$$k = k_0(\phi/\phi_0)^3, \tag{21}$$

where k_0 is the coal permeability at a stress-free state (m^2), and k is permeability corresponding to porosity ϕ.

Considering $abs[-(\varepsilon_v+p/K_s-\varepsilon_s-\alpha_T T)]\ll 1$ and according to Eq. (18), the simplified expression for porosity can be defined as

$$\phi\approx\phi_0 + (\alpha-\phi_0)[(\varepsilon_v + p/K_s-\varepsilon_s-\alpha_T T)-(\varepsilon_{v0} + p_0/K_s-\varepsilon_{s0}-\alpha_T T_0)]. \tag{22}$$

In this respect, the simplification from Eqs. (18) to (22) does not incur a large error, but it does significantly simplify the analysis. In this work, nevertheless, this simplification is never adopted because Eq. (18) can be easily handled during the numerical simulations.

Substituting Eqs. (19) and (20) into Eq. (14) yields the governing equation for gas flow through a coal seam with gas sorption and thermal effects included as

$$\begin{aligned}&\frac{1}{(T_{ar}+T)}\left[\phi + \frac{(\alpha-\phi)p}{K_s}\right]\frac{\partial p}{\partial t}-\left[\frac{\phi p}{(T_{ar}+T)^2} + \frac{p(\alpha-\phi)\alpha_T}{(T_{ar}+T)}\right]\frac{\partial T}{\partial t}\\ &\quad+\left[\frac{p_a\rho_c V_L}{T_a}-\frac{(\alpha-\phi)p\alpha_{sg}V_L}{T_{ar}+T}\right]\\ &\quad\times\left\{\begin{array}{l}\frac{P_L}{(p+P_L)^2}\exp\left(-\frac{c_2}{1+c_1p}(T+T_{ar}-T_t)\right)\frac{\partial p}{\partial t}\\ +\frac{p}{(p+P_L)}\exp\left(-\frac{c_2}{1+c_1p}(T+T_{ar}-T_t)\right)\frac{c_1c_2}{(1+c_1p)^2}(T+T_{ar}-T_t)\frac{\partial p}{\partial t}\\ -\frac{p}{(p+P_L)}\exp\left(-\frac{c_2}{1+c_1p}(T+T_{ar}-T_t)\right)\frac{c_2}{1+c_1p}\frac{\partial T}{\partial t}\end{array}\right\}\\ &\quad-\frac{1}{\mu}\left[\frac{\partial}{\partial x}\left(\frac{pk}{(T_{ar}+T)}\frac{\partial p}{\partial x}\right) + \frac{\partial}{\partial y}\left(\frac{pk}{(T_{ar}+T)}\frac{\partial p}{\partial y}\right)\right] = \frac{R}{M_g}Q_s-\frac{p(\alpha-\phi)}{(T_{ar}+T)}\frac{\partial\varepsilon_v}{\partial t}.\end{aligned} \tag{23}$$

where ϕ and k are still variables that will be substituted with Eqs. (17) and (21), respectively, in the numerical analysis.

2.3. Energy conservation

By neglecting the thermal-filtration effect, the total heat flux $\mathbf{q}_T$ is given by

$$\mathbf{q}_T = -\lambda_M\nabla T + \rho_g C_g\mathbf{q}_g(T_{ar}+T), \tag{24}$$

$$\lambda_M = (1-\phi)\lambda_s + \phi\lambda_g, \tag{25}$$

where $\mathbf{q}_T$ is thermal flux [$J\cdot s^{-1}\cdot m^{-2}$)], ρ_s is the mass density of the gas ($kg\cdot m^{-3}$), C_g is the gas specific heat constants at constant volume ($J\cdot kg^{-1}\cdot K^{-1}$), $\mathbf{q}_g$ is the Darcy velocity as expressed in Eq. (13), and λ_M, λ_s and λ_g are the thermal conductivities of coal, solid (rock) and gas components [$J\cdot s^{-1}\cdot m^{-1}\cdot K^{-1}$)], respectively. The first term on the right-hand side of Eq. (24) is the heat flux transmitted by conduction in the fluid–solid mixture, which is given by Fourier's law; the last term on the right-hand side of Eq. (24) represents the convective heat flux (the transport of enthalpy by gas flow through the pores). Due to the assumption of thermal equilibrium between the fluid and solid phases, thermal balance over an REV can be expressed in terms of a single equation neglecting the interconvertibility of thermal and mechanical energy (Biot, 1956; Tong et al., 2010; Zhou et al., 1998), which reads

$$\frac{\partial[(\rho C)_M(T_{ar}+T)]}{\partial t} + (T_{ar}+T)K_g\alpha_g\nabla\cdot\mathbf{q}_g + (T_{ar}+T)K\alpha_T\frac{\partial\varepsilon_v}{\partial t} = -\nabla\cdot\mathbf{q}_T \tag{26}$$

$$(\rho C)_M = \phi\left(\rho_g C_g\right) + (1-\phi)(\rho_s C_s), \tag{27}$$

where $(\rho C)_M$ is the specific heat capacity of the gas-filled solid medium, ρ_s is the mass density of the rock matrix ($kg\cdot m^{-3}$), and C_g and C_s are the gas and solid specific heat constants at constant volume ($J\cdot kg^{-1}\cdot K^{-1}$), respectively. K_g is the bulk modulus of the gas (Pa) and α_g ($\alpha_g=1/T$) is the thermal expansion coefficient of the gas under constant pore pressure and stress (K^{-1}). As defined by Tong et al. (2010), $K_g=p$ (in Pa) and $\alpha_g=1/T$ (in K^{-1}).

The first term on the left-hand side of Eq. (26) represents internal heat energy change rate per unit volume due to temperature change. The second term represents a heat sink due to thermal dilatation of the gas. The last term represents a heat sink due to thermal expansion of the medium. For a small variation of temperature (the temperature changes T are small compared to the absolute ambient temperature), $T_{ar}+T\approx T_{ar}$ and this term is identical to that given by Biot (1956). The second and third terms on the left-hand side of Eq. (26) represent the thermoporoelastic coupling in the heat energy balance equation (Zhou et al., 1998).

Assuming constant specific heats (C_s and C_g) and thermal conductivities (λ_s and λ_g) then substituting Eqs. (24), (25) and (27) into Eq. (26) yields

$$\begin{aligned}&(\rho C)_M\frac{\partial T}{\partial t} + C_s(T_{ar}+T)\frac{\partial[(1-\phi)\rho_s]}{\partial t} + C_g(T_{ar}+T)\frac{\partial\left(\phi\rho_g\right)}{\partial t} + (T_{ar}+T)K_g\alpha_g\nabla\cdot\mathbf{q}_g\\ &\quad+(T_{ar}+T)K\alpha_T\frac{\partial\varepsilon_v}{\partial t} = \lambda_M\nabla^2 T + \lambda_s\nabla(1-\phi)\cdot\nabla T + \lambda_g\nabla\phi\cdot\nabla T\\ &\quad-\rho_g\mathbf{q}_g C_g\nabla(T_{ar}+T)-C_g(T_{ar}+T)\nabla\cdot\left(\rho_g\mathbf{q}_g\right).\end{aligned} \tag{28}$$

As given by Zhou et al. (1998), the conservation of mass of the two phases in the REV yields

$$\frac{\partial[(1-\phi)\rho_s]}{\partial t} = 0 \tag{29}$$

$$\frac{\partial\left(\phi\rho_g\right)}{\partial t} = -\nabla\cdot\left(\rho_g \mathbf{q}_g\right) \tag{30}$$

Based on Eq. (18), the differentiation of ϕ with respect to the spatial coordinates x, y and z yields

$$\begin{aligned}\nabla\phi = {} & (\alpha-\phi)\left(\nabla\varepsilon_v + \frac{1}{K_s}\nabla p - \alpha_T\nabla T\right) \\ & + (\alpha-\phi)\frac{-\alpha_{sg}V_L}{p+P_L}\exp\left[-\frac{c_2}{1+c_1 p}(T_{ar}+T-T_t)\right] \\ & \times\left[\frac{c_1c_2p(T+T_{ar}-T_t)}{(1+c_1p)^2}\nabla p - \frac{c_2p}{1+c_1p}\nabla T + \frac{P_L}{p+P_L}\nabla p\right].\end{aligned} \tag{31}$$

Substituting Eqs. (11), (12), (13), (29), (30) and (31) into Eq. (28) yields

$$\begin{aligned}&(\rho C)_M\frac{\partial T}{\partial t} - (T_{ar}+T)K_g\alpha_g\nabla\cdot\left(\frac{k}{\mu}\nabla p\right) + (T_{ar}+T)K\alpha_T\frac{\partial\varepsilon_v}{\partial t} \\ &= \lambda_M\nabla^2 T + \frac{\rho_{ga}pT_aC_g}{p_a(T_{ar}+T)}\frac{k}{\mu}\nabla p\nabla T + \left(-\lambda_s+\lambda_g\right)(\alpha-\phi)\left(\nabla\varepsilon_v\nabla T + \frac{1}{K_s}\nabla p\nabla T - \alpha_T\nabla T\nabla T\right) \\ &\quad + \left(-\lambda_s+\lambda_g\right)(\alpha-\phi)\times\frac{-\alpha_{sg}V_L}{p+P_L}\exp\left[-\frac{c_2}{1+c_1p}(T_{ar}+T-T_t)\right] \\ &\quad \times\left[\frac{c_1c_2p(T+T_{ar}-T_t)}{(1+c_1p)^2}\nabla p\nabla T - \frac{c_2p}{1+c_1p}\nabla T\nabla T + \frac{P_L}{p+P_L}\nabla p\nabla T\right].\end{aligned} \tag{32}$$

Eqs. (7), (23) and (32) constitute a set of fully coupled nonlinear equations governing the thermoporoelastic response of gas flow in a saturated coal seam. The equations account for the multiphysics of this work, including thermodynamically coupled heat and mass transfer, mechanical and thermal compressibility of the constituents, and most importantly convective heat flow.

Considering $(1-\phi)\lambda_s >> \phi\lambda_g$ and $\lambda_M \approx (1-\phi)\lambda_s \approx \lambda_s$, Eq. (32) can be simplified as

$$\begin{aligned}(\rho C)_M\frac{\partial T}{\partial t} - (T_{ar}+T)K_g\alpha_g\nabla\cdot\left(\frac{k}{\mu}\nabla p\right) + (T_{ar}+T)K\alpha_T\frac{\partial\varepsilon_v}{\partial t} &= \lambda_M\nabla^2 T \\ + \frac{\rho_{ga}pT_aC_g}{p_a(T_{ar}+T)}\frac{k}{\mu}\nabla p\nabla\mathrm{T}&\end{aligned} \tag{33}$$

Different physical processes generally progress at different rates. Thermal processes are rather slow due to the high heat capacity of the solid; gas processes progress relatively faster in fractures and significantly slower in the intact solid. The propagation rate of elastic stresses may be treated as spontaneous when compared with these timescales.

The above governing equations, especially the gas flow equation and energy conservation equation are nonlinear second-order partial differential equations (PDEs) in space and first order in time. These equations are not easy to solve theoretically due to the nonlinearity in both the space and time domain, therefore they are implemented into COMSOL Multiphysics (COMSOL, 2008), and solved by the finite element method.

3. Numerical simulation on gas drainage

A representative model geometry is shown in Fig. 1, containing a wellbore with the diameter of 0.1 m set centrally within a 100 m × 100 m × 5 m domain. The external boundary is restrained from boundary-normal displacements and insulated for gas and thermal transport. The initial gas pressure in the coal seam $p\,(t=0)=3.0$ MPa, and the initial value of the temperature increment $T\,(t=0)=10$ K. For the wellbore, gas pressure $p_w=0.1$ MPa, temperature $T_w=0$ K. Other related parameters used in the numerical simulations are listed in

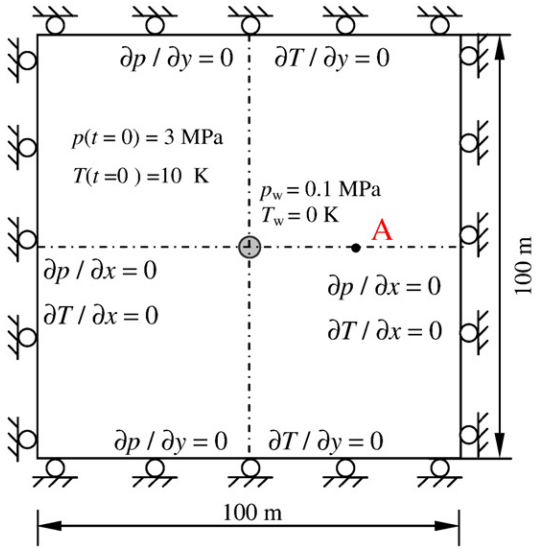

Fig. 1. Model setup for a centrally located gas production well within a square reservoir block.

Table 1. Furthermore, the coal seam is assumed to be in a state of plane stress (with no change in elastic stress in the vertical direction), and quasi-static mechanical equilibrium.

A total of four scenarios (scenarios I, II, III and IV as listed in Table 2) are simulated in order to examine the effect of gas pressure, temperature, and gas adsorption on the response of the coal seam. Specifically, the term αp in Eq. (4) is studied in scenario I to investigate the effect of gas pressure on the deformation of the coal matrix. Scenario II supplements scenario I, where the term $\alpha_T T$ is accommodated to study the effect of temperature change on matrix deformation. Scenario III focuses on the effect of temperature on gas adsorption defined in terms of the Langmuir relation $\exp\left[-\frac{c_2}{1+c_1p}(T_{ar}+T-T_t)\right]$. Scenario IV examines the effect of gas desorption on the matrix deformation term, ε_s.

Furthermore, five scenarios, V–IX as listed in Table 3, are defined to clarify the effect of coal seam deformation and gas flow on thermal

Table 1
Parameters used in the numerical simulation.

Variable	Parameter	Value	Unit
E	Young's modulus of coal	2713	MPa
E_s	Young's modulus of coal grains	4070	MPa
ν	Poisson's ratio of coal	0.339	
ρ_c	Density of coal	1.25×103	$Kg\cdot m^{-3}$
ρ_{ga}	Density of methane at standard condition	0.717	$Kg\cdot m^{-3}$
α_{sg}	Coefficient for sorption-induced volumetric strain	0.06	$Kg\cdot m^{-3}$
ϕ_0	Initial porosity of coal	0.01	
k_0	Initial permeability of coal	1×10^{-15}	m^2
μ	Methane dynamic viscosity	1.84×10^{-5}	$Pa\cdot s$
V_L	Langmuir volume constant	0.043	$m^3\cdot Kg^{-1}$
P_L	Langmuir pressure constant	1.57	MPa
c_1	Pressure coefficient	0.07	MPa^{-1}
c_2	Temperature coefficient	0.02	K^{-1}
T_0	Absolute reference temperature	300	K
T_t	Reference temperature for desorption/adsorption test of gas (K)	300	K
Q_s	Source term	0	$kg\cdot m^{-3}\cdot s^{-1}$
α_T	Volumetric thermal expansion of the solid matrix coefficient	2.4×10^{-5}	K^{-1}
λ_s	Thermal conductivity of coal	0.2	$J\cdot/(m\cdot s\cdot K)$
C_s	Specific heat capacity of coal	1.25×10^3	$J/\cdot(kg\cdot K)$
C_g	Specific heat capacity of gas	1.625×10^3	$J/\,(kg\cdot K)$
p_a	Pressure at standard condition	0.101325	MPa
T_a	Temperature at standard condition	273	K

Table 2
List of four simulation scenarios to examine the effect of gas pressure, temperature, and gas adsorption on coal seam deformation.

	Scenario I	Scenario II	Scenario III	Scenario IV
Effect of gas pressure on matrix deformation, term αp	√	√	√	√
Effect of temperature change on matrix deformation, term $\alpha_T T$		√	√	√
Effect of temperature on gas adsorption, term $exp\left[-\frac{c_2}{1+c_1 p}(T_{ar}+T-T_t)\right]$			√	√
Effect of gas desorption on matrix deformation, term ε_s				√

transport. This utilizes the simplified term (Section 2.3) $\lambda_M=(1-\phi)\lambda_s+\phi\lambda_g$ as λ_s in the energy conservation equation. The fidelity of this simplification is examined.

3.1. Evolution of coal porosity

3.1.1. Comparison between Scenarios I and II

Compared with the gas-pressure-induced porosity changes of scenario I alone, the change of porosity in scenario II is caused by both the gas pressure and temperature gradients. The distribution of porosity and gas pressure radially outwards from the wellbore under scenarios I and II are shown in Fig. 2.

As shown in Fig. 2, the initial porosity at the wellbore is a little lower than ϕ_0 due to the effect of the boundary condition. At 20 m from the wellbore in scenario I the porosity has a slight reduction (about 2%) (i.e., $\phi/\phi_0=0.978$) at $t=1e10$ s, compared with the initial condition ($\phi/\phi_0=1$) resulting from the compaction of the coal seam due to an increase in effective stresses during gas drainage. To the contrary, the relative porosity at $t=1e10$ s in scenario II ($\phi/\phi_0=0.986$), is slightly increased relative to that in Scenario I, denoting the minor increase of porosity due to the temperature gradient. As can be seen from Eq. (18), the effect of temperature increase on porosity is opposite to that of the gas pressure. However, as time elapses, for example, at $t=1e8$ s, gas pressures under the two scenarios are similar, which confirms that the temperature-induced porosity (or permeability) variation has only a minor influence on gas flow.

The coal seam expands with the elevation in temperature, however, because deformation is restrained due to confinement of the external boundary, the resultant compressive stress and strain to reduce the permeability of the coal seam. With the progress in gas drainage, temperature of the coal seam declines gradually, abating the temperature-induced effect and leading to an increase in permeability of the coal seam.

Table 3
Five scenarios considered in the numerical simulation in order to examine the effect of coal seam deformation and gas flow on thermal processes in coal.

	Scenario V	Scenario VI	Scenario VII	Scenario VIII	Scenario IX
Heat diffusion, simplified term $\lambda_M=\lambda_s$	√				
Heat diffusion, term $\lambda_M=(1-\phi)\lambda_s+\phi\lambda_g$		√	√	√	√
Heat sink due to thermal dilatation of the gas, term $(T_0+T)K_g\alpha_g\nabla\cdot\left(\frac{k}{\mu}\nabla p\right)$			√	√	√
Heat sink due to thermal expansion of solid medium, term $(T_0+T)K\alpha_T\frac{\partial\varepsilon_v}{\partial t}$				√	√
Convective heat flux, term $\frac{\rho_{g0}T_0C_g}{\mu p_a}\nabla\cdot(kp\nabla p)$					√

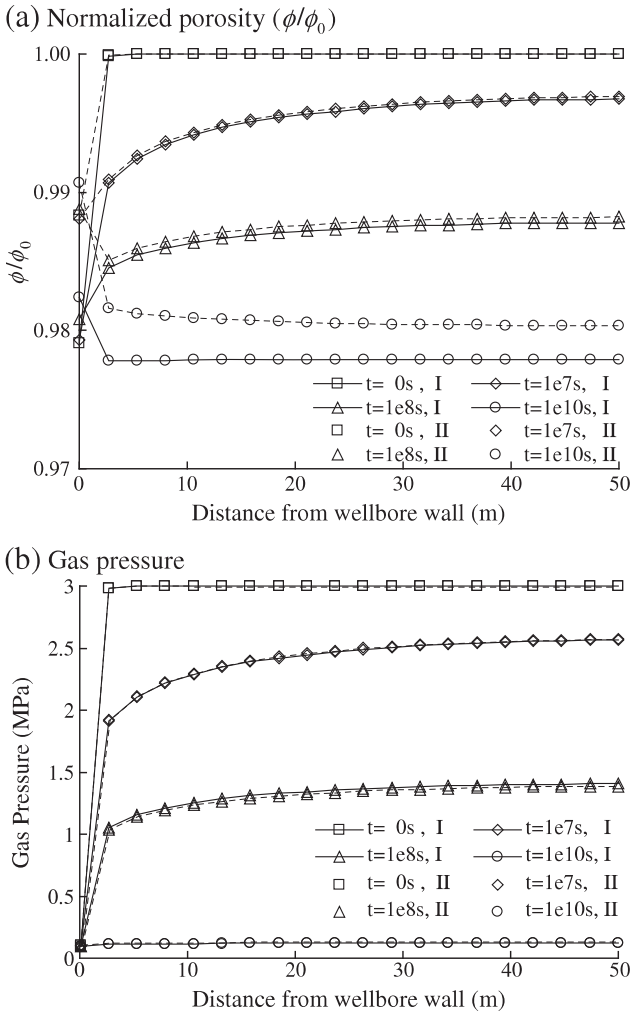

Fig. 2. Variation of porosity and gas pressure with distance from the wellbore wall under scenarios I and II.

3.1.2. Comparison between Scenarios II and III

Variations of porosity and gas pressure with distance from the wellbore under scenarios II and III are shown in Fig. 3. At the same time (for example, $t=1e8$ s) the relative porosity (ϕ/ϕ_0) in scenario III is smaller in comparison to that in scenario II, as is also the gas pressure. Since the effect of porosity on gas pressure is minor, as discussed in Section 3.1.1, the difference in gas pressure between scenarios II and III originates in the temperature-induced gas desorption. The initial gas pressures are identical for these two scenarios, but gas contents are not. For gas flow within the coal seam, gas content, considered as a source term in Eq. (23), may vary with absorption or desorption of gas from coal seam. Due to the reduction in gas content caused by the temperature increase, the initial gas content in scenario III is lower than that in scenario II even though the initial gas pressures are identical.

As shown in Fig. 4, the accumulative gas production curves for scenarios I and II overprint, indicating that the effect of temperature change on the matrix deformation does not change gas production. By contrast, the difference between scenarios II and III are distinct. Even though the two curves are overprinted in the interval between $t=1e5$ s and $t=1e7$ s, they are separated after $t=1e07$ s, reflecting that the production in scenario III is lower than those in both scenarios I and II. This explains why the gas pressure in scenario III is lower than that in scenarios I and II.

Similar to Fig. 4, the gas recovery curves of scenarios I and II also overprint in Fig. 5. However, it is noticeable that the gas recovery in

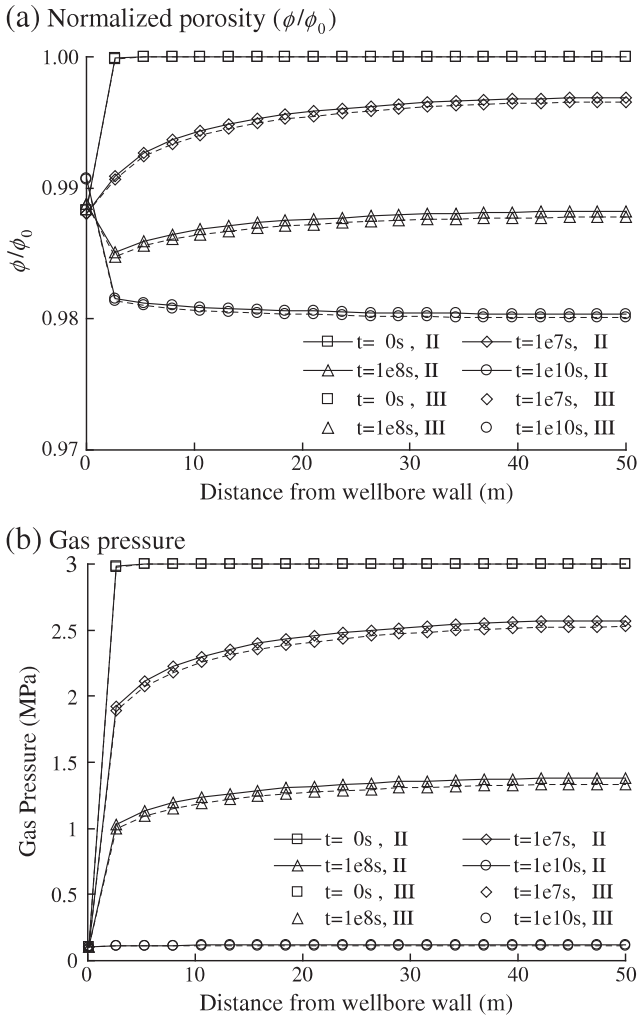

Fig. 3. Variation of porosity and gas pressure with distance from the wellbore under scenarios II and III.

scenario III is greater at the beginning of gas drainage (before $t = 1e10$ s), but becomes lower after $t = 1e10$ s than that in scenarios I and II.

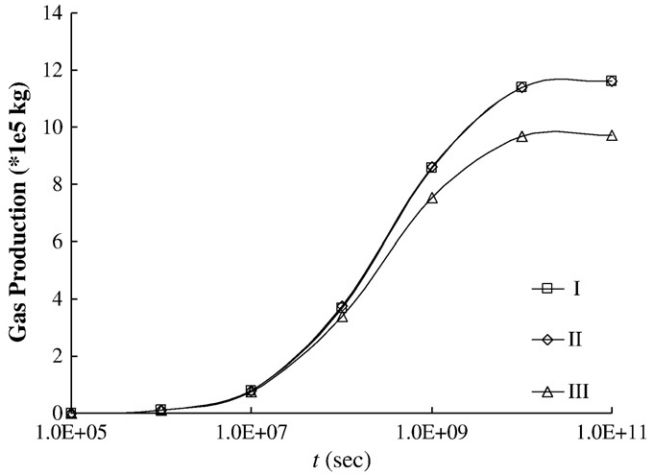

Fig. 4. Gas production from the coal seam until $t = 1e11$ s under scenarios I, II and III.

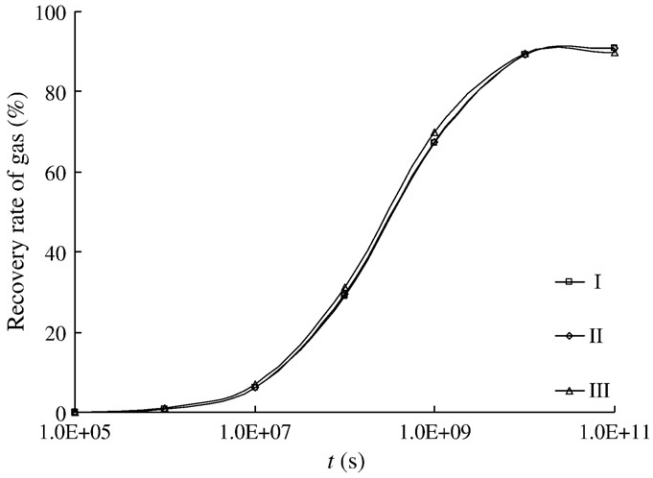

Fig. 5. Gas recovery rate from the coal seam until $t = 1e11$ s under scenarios I, II and III.

As shown in Fig. 6 the temperature in scenario III is higher than that in scenario II, indicating that temperature decline slows down after the gas drains from coal seam. This actually reflects the effect of gas flow on thermal transport, which will be detailed in the next section.

3.1.3. Comparison with Scenario IV

Fig. 7 indicates that coal porosity changes significantly during gas production when the desorption-induced matrix deformation is taken into account in scenario IV. Therefore, the effect of the desorption-induced deformation on porosity is the most prominent factor compared to those of gas pressure (Scenario I) and temperature gradient (scenarios II and III). In contrast to the porosity decrease with gas drainage in scenarios II and III, the desorption-induced matrix deformation considered in scenario IV results in a porosity increase. If this effect is not considered, as for scenarios I, II and III, the opposite tendencies are predicted. This indicates that it is important to consider the gas-desorption-induced deformation in order to correctly predict gas flow.

When a higher gas pressure of 8 MPa is applied as the initial condition for the model shown in Fig. 1, the porosity variation with gas drainage is shown in Fig. 8. It is found that the porosity variation in scenarios I, II and III retains its original trend; however, the porosity in scenario IV declines with gas drainage until a gas pressure of about 2.5 MPa and then increases. Based on Eq. (22), it is apparent that the

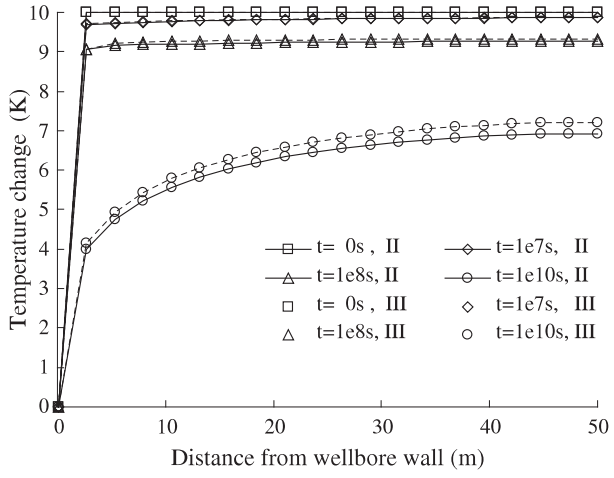

Fig. 6. Variation of temperature with time at different distances away from the wellbore under scenarios II and III.

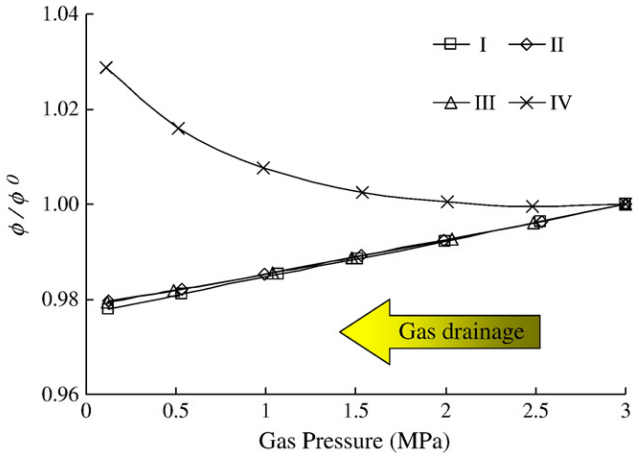

Fig. 7. Variation of porosity at point A (25 m from the wellbore) during gas drainage in scenarios I, II, III and IV.

porosity change is dependent on four components. These are volumetric strain ε_v, gas-induced fluid deformation p/K_s, desorption-induced volumetric matrix strain ε_s, and thermal expansion αT. Fig. 8 (b) shows the response of these four components in contributing to the porosity change. Their contributions to the porosity change vary distinctly, i.e., volumetric strain ε_v never significantly affects the porosity; gas-induced solid deformation p/K_s induces a linear decline in porosity; both desorption-induced volumetric matrix strain ε_s and thermal expansion αT induces increasing porosity, although the thermal expansion-induced porosity is slight. Altogether, porosity first decreases during gas drainage reaching a minimum at a gas pressure of about 2.5 MPa and then rebounds to a magnitude close to its initial value.

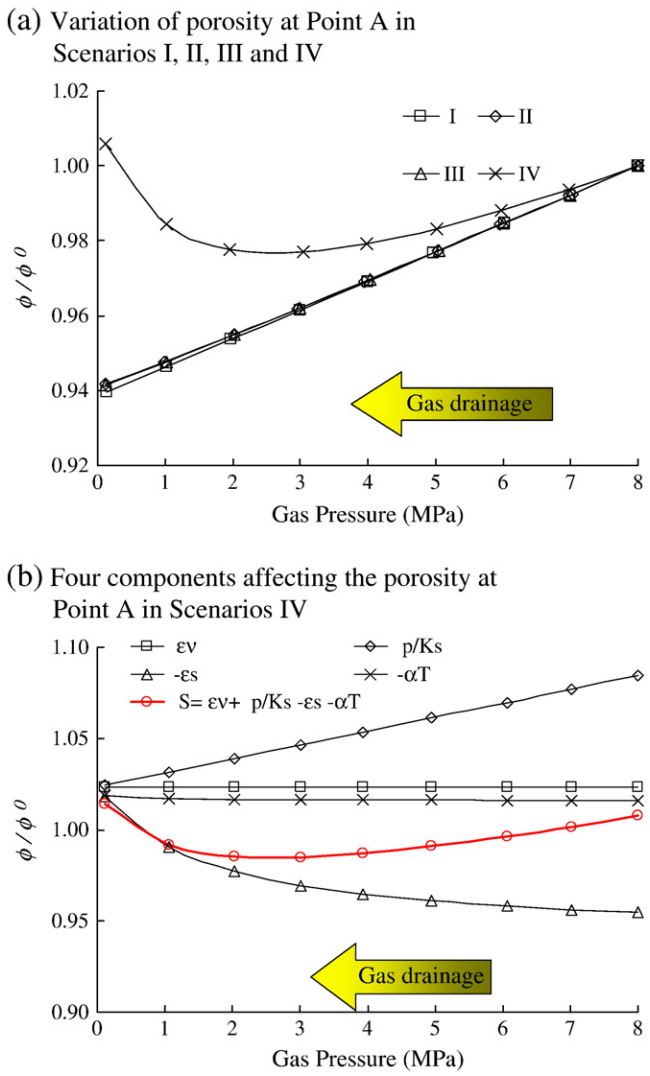

Fig. 8. Variation of porosity at point A (25 m from the wellbore) in scenarios I, II, III and IV when the initial gas pressure is specified as 8 MPa.

3.2. Effect on the thermal transport

As shown in Fig. 9, due to scenarios V and VI, the temperature distributions are overprinted, indicating that the simplification as stated in Eq. (33) is feasible if the thermal transport is described as due the thermal diffusion only. In these two scenarios (V and VI), at $t = 1e10$ s, the temperature decreases by only 1.2 K at the position that is 50 m away from the wellbore wall. By contrast, if the heat sink due to thermal dilatation of the gas is also taken into account (in scenario VII), at $t = 1e10$ s and in the same position, a temperature decrease of 2.8 K is predicted. Excepting this, the temperature curves in scenarios VIII and IX almost overlap with that for scenario VII, indicating that the effects of solid deformation and convective heat flux is so small that they can be neglected. Therefore, under the conditions considered in this study, in contrast to other factors that are taken into account, the heat sink due to thermal dilatation of the gas (termed as $(T_0 + T)K_g\alpha_g\nabla\cdot\left(\frac{k}{\mu}\nabla p\right)$ in Eq. (32)) is the most prominent factor in altering the temperature of the coal seam. In this regard, the temperature variation as shown in Fig. 6 is the comprehensive contribution of all the above-mentioned factors.

4. Conclusions

A fully coupled model representing coal deformation, gas transport and thermal transport is developed and implemented. The model is applied to examine the complex coal–gas interactions under variable temperatures. Based on the results of a series of numerical simulations under different scenarios, the following conclusions are drawn:

(1) A general porosity model is proposed to represent coal seams, which accommodates the influences of gas pressure, thermally induced solid deformation, thermally induced gas adsorption and gas-desorption-induced solid deformation. The model can characterize the evolution of porosity during fully coupled gas flow, geomechanics and heat transfer processes. Under the boundary and initial conditions specified in this work, the gas-

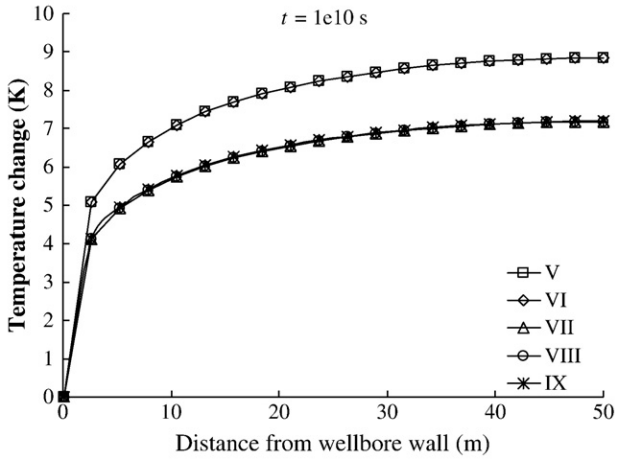

Fig. 9. Variation of temperature at different distances away from the wellbore under scenarios V, VI, VII and VIII at $t = 1e10$ s.

desorption-induced deformation is more salient than the other three factors in affecting the porosity.

(2) In this work, among the factors of thermal expansion of the solid and the gas, convective heat flux, in addition to the thermal diffusion, the heat sink due to thermal dilatation of gas is the most prominent factor in altering the temperature of the coal seam. In this respect, the temperature variation is the most comprehensive contribution of all above-mentioned factors.

In this respect, in order to evaluate gas flow correctly and to clarify the mechanisms associated with coupled coal–gas interaction during gas flow in coal seams, it is of paramount importance to take the all the related factors into account in the numerical simulations. It should also be noted that, in this work, the coal seam is still assumed elastic. The effects of mining-induced damage, as well as its contribution to fully coupled processes, remain to be quantified.

Acknowledgements

This work was funded by the National Science Foundation of China (Grant Nos. 50874024, 50934006, 50911140284 and 51010105043), the National Basic Research Program ("973 Program") of China (Grant No. 2007CB209405), the Fok Ying Tung Education Foundation (Grant No.122023), and the Fundamental Research Funds for the Central Universities of China (Grant Nos. N090501001, N090101001, N100701001 and N100601004). This support is gratefully acknowledged. The authors are grateful to the reviewers for discerning comments on this paper.

References

Ayers, W.B., 2002. Coalbed methane systems, resources, and production and a review of contrasting cases from the San Juan and Powder River basins. AAPG Bulletin 86 (11), 1853–1890.

Biot, M.A., 1956. Thermoelasticity and irreversible thermodynamics. Journal of Applied Physics 27 (3), 240–253.

Brunauer, S., 1943. Sorption of Gases and Vapors. Princeton University Press, Princeton, NJ. 540 pp.

Bustin, R.M., Clarkson, C.R., 1998. Geological controls on coalbed methane reservoir capacity and gas content. International Journal of Coal Geology 38, 3–26.

COMSOL, A.B., 2008. COMSOL Multiphysics Version 3.5: User's Guide and Reference Guide. www.comsol.com.

Creedy, D.P., 1991. An introduction to geological aspects of methane occurrence and control in British deep coal mines. Quarterly Journal of Engineering Geology 24, 209–220.

Cui, X., Bustin, R.M., 2005. Volumetric strain associated with methane desorption and its impact on coalbed gas production from deep coal seams. AAPG Bull 89, 1181–1202.

Detournay, E., Cheng, A.H.D., 1993. Fundamentals of poroelasticity. In: Fairhurst, C. (Ed.), Comprehensive rock engineering, vol. 2. Pergamon, Oxford, pp. 113–171.

Durucan, S., Ahsan, M., Shi, J.Q., 2005. Matrix shrinkage and swelling characteristics of European coals. Energy Procedia 1, 3055–3062.

Gunter, W.D., Gentzis, T., Rottenfuser, B.A., Richardson, R.J.H., 1997. Deep coalbed methane in Alberta, Canada: A fossil resource with the potential of zero greenhouse gas emissions. Energy Conversion Management 38 (Suppl), 217–222.

Han, W.S., Stillman, G.A., Lu, M., Lu, C., McPherson, B.J., Park, E., 2010. Evaluation of potential nonisothermal process and heat transport during CO_2 sequestration. Journal of Geophysical Research 115 (B07209).

Harpalani, S., Chen, G., 1997. Influence of gas production induced volumetric strain on permeability of coal. Geotechnical and Geological Engineering 15, 3030–3325.

Harpalani, S., Schraufnagel, R., 1990. Shrinkage of coal matrix with release of gas and its impact on permeability of coal. Fuel 69, 551–556.

Izadi, G., Wang, S., Elsworth, D., Liu, J., Wu, Y., Pone, D., 2011. Permeability evolution of fluid-infiltrated coal containing discrete fractures. International Journal of Coal Geology 85, 201–211.

Lama, R.D., Bodziony, J., 1998. Management of outburst in underground coal mines. International Journal of Coal Geology 35, 83–115.

Levy, J., Day, S.J., Killingley, J.S., 1997. Methane capacity of Bowen Basin coals related to coal properties. Fuel 74, 1–7.

Liang, B., 2000. Study on temperature effects on the gas absorption performance (in Chinese). Journal of Heilongjiang Mining Institute 10 (1), 20–22.

Litwiniszyn, J., 1985. A model for the initiation of coal–gas outbursts. International Journal of Rock Mechanics and Mining Sciences and Geomechanical Abstracts 22 (1), 39–46.

Mazumder, S., Wolf, K.H., 2008. Differential swelling and permeability change of coal in response to CO_2 injection for ECBM. International Journal of Coal Geology 74, 123–138.

Metz, B., 2005. IPCC Special Report on Carbon Dioxide Capture and Storage. Cambridge University Press, Cambridge, New York, NY, USA.

Noack, K., 1998. Control of gas emissions in underground coal mines. International Journal of Coal Geology 35, 57–82.

Palmer, I., Mansoori, J., 1996. How permeability depends on stress and pore pressure in coalbeds. 1996 SPE Annual Technical Conference and Exhibition, Denver, CO. SPE Paper No. 36737.

Reichle, D., Houghton, J., Kane, B., 1999. Carbon sequestration: Research and development. U.S. DOE report. .

Scott, A.R., 2002. Hydrogeologic factors affecting gas content distribution in coal beds. International Journal of Coal Geology 50, 363–387.

Shi, J.Q., Durucan, S., 2001. Drawdown induced changes in permeability of coalbeds: A new interpretation of the reservoir response to primary recovery. Transport in Porous Media 56, 1–16.

Tong, F.G., Jing, L., Zimmerman, R.W., 2010. A fully coupled thermo-hydro-mechanical model for simulating multiphase flow, deformation and heat transfer in buffer material and rock masses. International Journal of Rock Mechanics and Mining Sciences 47 (2), 205–217.

van Bergen, F., Pagnier, H., Krzystolik, P., 2006. Field experiment of enhanced coalbed methane-CO_2 in the upper Silesian basin of Poland. Environmental Geosciences 13, 201–224.

Zhang, H.B., Liu, J., Elsworth, D., 2008. How sorption-induced matrix deformation affects gas flow in coal seams: A new FE model. International Journal of Rock Mechanics & Mining Sciences 45 (8), 1226–1236.

Zhou, Y., Rajapakse, R., Graham, J., 1998. A coupled thermoporoelastic model with thermo-osmosis and thermal-filtration. International Journal of Solids Structures 35 (34–35), 4659–4683.

Zhu, W.C., Liu, J., Sheng, J.C., Elsworth, D., 2007. Analysis of coupled gas flow and deformation process with desorption and Klinkenberg effects in coal seams. International Journal of Rock Mechanics and Mining Sciences 44 (7), 971–980.